

Molecular gas towards G18.8+1.8

J. Vasquez^{1,2*}, M. Rubio³, C.E. Cappa^{1,2*}, and N. U. Duronea²

¹ Facultad de Ciencias Astronómicas y Geofísicas, Universidad Nacional de La Plata, Paseo del Bosque s/n, 1900 La Plata, Argentina
e-mail: pete@iar.unlp.edu.ar

² Instituto Argentino de Radioastronomía, C.C. 5, 1894 Villa Elisa, Argentina

³ Departamento de Astronomía, Universidad de Chile, Casilla 36-D, Santiago, Chile

Received September 15, 1996; accepted March 16, 1997

ABSTRACT

Aims. This work aims at investigating the characteristics of the molecular gas associated with the nebula G18.8+1.8, linked to the Wolf-Rayet star HD 168206 (WR 113), and its relation to other components of its local interstellar medium.

Methods. We carried out molecular observations of the $^{12}\text{CO}(J = 1 - 0)$ and $(J = 2 - 1)$ lines with angular resolution of $44''$ and $22''$ using the SEST telescope. Complementary NANTEN data of the $^{12}\text{CO}(1-0)$ line were also used. The dust emission was analyzed using Spitzer-IRAC images at $8.0\ \mu\text{m}$, and WISE data at $3.4\ \mu\text{m}$, $4.6\ \mu\text{m}$, and $12.0\ \mu\text{m}$.

Results. The SEST data allowed us to identify a molecular component (Cloud 3) having velocities in the interval from $\sim +30$ to $+36\ \text{km s}^{-1}$ which is most probably linked to the nebula. Morphological and kinematical properties suggest that Cloud 3 constitute a wind-blown molecular half-shell, which expands around WR 113. The ratio $R_{2-1/1-0}$ and excitation temperatures indicate that the molecular gas is being irradiated by strong UV radiation. The location of the inner optical ring in the outer edge of Cloud 3 suggests that the stars SerOB2-1, -2, -3, -63, and -64 are responsible for the ionization of Cloud 3 and the inner ring nebula. A comparison between the spatial distribution of the molecular gas and the PAH emission at $8\ \mu\text{m}$ indicates the existence of a PDR between the ionized and the molecular gas.

A search for candidate young stellar objects (YSOs) in the region around G18.8+1.8 based on available 2MASS, MSX, IRAS, and Spitzer-IRAC catalogs resulted in the detection of about sixty sources, some of them projected onto Cloud 3. Two small spots of clustered candidates YSOs are projected near the outer border of Cloud 3, although a triggered stellar formation scenario is doubtful.

Key words. ISM: bubbles – ISM: individual object: G18.8+1.8 – stars: Wolf-Rayet – stars: individual: WR 113

1. Introduction

Most massive star formation in our Galaxy occurs in Giant Molecular clouds (GMC) where, in general, the star formation is developed in groups like stellar clusters or OB associations. These groups can contain hundreds of OB stars, including massive young stellar objects (MYSOs) and evolved massive stars. Since OB associations directly influence the evolution of their environs, it is important to study how this interaction occurs in different interstellar environments. Massive stars interact with the interstellar medium (ISM) through their intense ultraviolet (UV) radiation field ($h\nu > 13.6\ \text{eV}$) and via strong stellar winds. UV photons ionize the surrounding gas creating HII regions and dissociate the molecular gas originating photodissociation regions (PDRs), while the second mechanism alters the structure of HII regions sweeping up the circumstellar material and creating interstellar bubbles (IB) (Cappa et al. 2005).

SerOB2 is a rich OB association located at $RA, Dec.(J2000) \simeq (18^h 18^m 00^s, -11^\circ 36' 36'')$, at a distance of $1.9 \pm 0.3\ \text{kpc}$ (Forbes 2000), about 70 pc above the Galactic plane. Forbes (2000) performed a very interesting spectrophotometric study of this association and analyzed its connection to a narrow column of hot gas emerging from the HII region Sh2-54 perpendicularly to the Galactic plane, known as the thermal “chimney” (Mueller et al. 1987). From the original set of stars (~ 500) taken for the analysis, only 107 were considered to be probable members of SerOB2 (see Table 5 from Forbes

2000). Ser OB2 contains a number of massive stars including the eclipsing binary system CV Ser (Massey & Niemela 1981), the Of-type binary HD 166734 (Conti et al. 1980), the O-type multiple star HD 167971 (MY Ser ; Leitherer et al. 1987), and the O5.5Vf star HD 168112.

Our aim in this paper is to investigate the existence of molecular gas in the environs of CV Ser and other possible members of SerOB2 based on high angular resolution SEST observations performed in the $^{12}\text{CO}(1-0)$ and $^{12}\text{CO}(2-1)$ lines, complemented with medium angular resolution CO (1-0) data from the NANTEN telescope and infrared images in the mid infrared (MIR).

1.1. Background of CV Ser and its close environs

The brightest component of CV Ser is the Wolf-Rayet star WR 113 (\equiv HD 168206, WC8d+O8-9IV, van der Hucht 2001). Table 1 summarizes the main parameters of WR 113: coordinates, spectral classification, visual absorption A_v , spectrophotometric distance, mass loss rate \dot{M} , and terminal velocity v_∞ .

Gonzalez & Rosado (1984) discovered a double optical structure of $4'$ and $9'$ in radius around the WR star and suggested that the outer ring, which is poorly defined, was formed by the WR star or its massive progenitor and is presently being photoionized by the O5.5Vf star HD 168112 (at $RA, Dec.(J2000) = (18^h 18^m 40.8^s, -12^\circ 06' 23.4'')$, also belonging to Ser OB2 and located to the southwest of the ring nebula. Esteban & Rosado (1995) observed the inner ring in $[\text{NII}] \lambda\lambda 6548, 6584$, $[\text{SII}]$

* Member of Carrera del Investigador, CONICET, Argentina

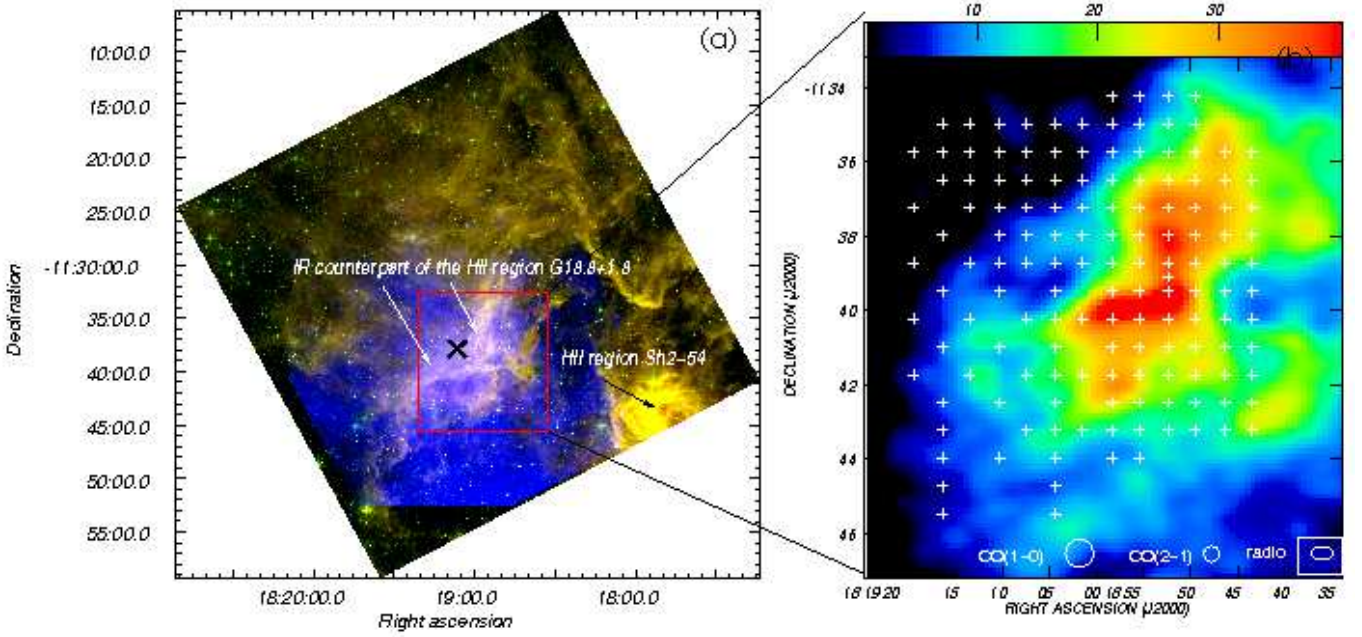


Fig. 1. *Left panel:* Superposition of the IRAC images at $8.0 \mu\text{m}$ (red) and $5.6 \mu\text{m}$ (green) with the $\text{H}\alpha$ emission (blue), of a section of the HII region Sh2-54 including the environs of WR 113. The cross marks the position of the WR star. *Right panel:* VLA image at 1465 MHz showing the ionized ring. The crosses mark the positions of the 143 points observed in ^{12}CO lines. The colour scale goes from 1 to 40 mJy beam^{-1} . The synthesized beam of the radio continuum observations and the beams of the molecular data are indicated in the bottom part of the image.

$\lambda 6717, 6731$, $\text{H}\alpha$ $\lambda 6563$, and $\text{H}\beta$ $\lambda 4861$. They determined that the velocity of the ionized gas is in the range $[\sim +27, \sim +39]$ km s^{-1} , which corresponds to a kinematical distance of 2.0 ± 0.2 kpc, according to circular galactic rotation models (e.g. Brand & Blitz 1993). A similar velocity of $+27 \text{ km s}^{-1}$ was found from radio recombination lines by Lockman (1989). Esteban & Rosado (1995) concluded that photoionization is the main source of excitation of the inner ring, being the WR star the main responsible. Following the classification by Chu (1991) for WR ring nebulae, they classified the inner nebula as R_s type, because it does not present evidence of expansion and its morphology is shell-structured.

The left panel of Fig. 1 shows a superposition of the IRAC images at $8.0 \mu\text{m}$ (in red) and $5.6 \mu\text{m}$ (green), with the $\text{H}\alpha$ emission (blue) of the ring nebula linked to CV Ser. The strong emission at RA, Dec.(J2000) = $(18^{\text{h}}18^{\text{m}}00^{\text{s}}, -11^{\circ}44')$ corresponds to the HII region Sh2-54. The bright filament to the west and south of the binary system, which is indicated by the cross symbol, corresponds to the inner structure of 4' in radius. This structure displays strong emission both in the $\text{H}\alpha$ line and in the mid-infrared.

The right panel of Fig. 1 displays the radio continuum emission distribution at 1465 MHz, as observed by Cappa et al. (2002) using the Very Large Array (VLA) in DnC configuration with a synthesized beam of $30''$. The radio continuum source was first identified as G18.8+1.8 by Goss & Day (1970) at 2.7 GHz. The high angular resolution VLA data allowed to detect radio counterparts of both the inner and outer rings. Adopting a distance of 2.0 ± 0.6 kpc, Cappa et al. (2002) obtained ionized masses and electron densities of $20 \pm 10 M_{\odot}$ and $180 - 500 \text{ cm}^{-3}$, respectively, for the inner shell, and $90 M_{\odot}$ and 40 cm^{-3} , respectively, for the outer shell. From the IR-radio continuum relation, they confirmed the thermal nature of the nebula. Adopting a ra-

Table 1. Main parameters of WR 113

RA, Dec.(J2000)	$(18^{\text{h}}19^{\text{m}}7.36^{\text{s}}, -11^{\circ}37'59''.20)$
Spectral classification	WC8d+O8-O IV
A_v (mag)	3.23 ± 0.1^a
d (kpc)	$1.8^a, 2.0^b, 2.5^{e,f}$
\dot{M} ($10^{-5} M_{\odot} \text{ yr}^{-1}$)	$< 5.6^g, 2.0 \pm 0.3^h, 2.4^f$
v_{∞} (km s^{-1})	$1400^i, 1890^j$

Notes: (a) van der Hucht (2001), (b) Conti & Vacca (1990), (e) Esteban & Rosado (1995), (f) Nugis & Lamers (2000), (g) Leitherer et al. (1997), (h) Lamontagne et al. (1996), (i) Koesterke & Hamann (1995), (j) Nugis et al. (1998).

dus $R_s = 2.3$ pc for the inner ring and an expansion velocity $v_{exp} = 5 - 10 \text{ km s}^{-1}$, the derived dynamical age $t_d = (1.3 - 2.5) \times 10^5$ yr suggests that the inner shell originated in the action of the stellar wind of the current WR phase.

A search for OB stars within a region $12'$ in size centered on the WR star indicated that other excitation sources are present in this region in addition to the binary system. Ser OB2-1, -2, and -3 are confirmed members of the OB association, while Ser OB2-63, and -64 are potential members (see Table 5 from Forbes 2000). Their coordinates and (B-V) and (U-B) colors are listed in Table 2.

In our study, in agreement with Forbes (2000), we adopt a distance of 2.0 ± 0.6 kpc. This value is also in agreement with the cataloged distances of the WR star (see Table 1)

2. SEST observations and complementary data

High angular resolution $^{12}\text{CO}(J = 1 \rightarrow 0)$ and $^{12}\text{CO}(J = 2 \rightarrow 1)$ data at 115 and 230 GHz, respectively, were obtained with the

Table 2. Other excitation sources identified in the environs of CV Ser.

	RA <i>J</i> (2000)	DEC. <i>J</i> (2000)	(<i>B</i> - <i>V</i>)	(<i>U</i> - <i>B</i>)
SerOB2-1	18 18 36.9	-11 40 57.8	1.32	0.01
SerOB2-2	18 18 39.9	-11 43 07.3	1.27	0.06
SerOB2-3	18 18 42.4	-11 43 54.8	1.25	0.11
SerOB2-63	18 18 53.4	-11 44 10.1	0.45	0.30
SerOB2-64	18 19 05.0	-11 42 58.3	0.81	0.22

Notes: from Forbes (2000).

15m Swedish-European Submillimetre Telescope (SEST), at La Silla, Chile during two observing runs in February 2002 and March 2003. The half-power beam-width of the telescope was 44'' and 22'' at 115 and 230 GHz, respectively. A high resolution acousto-optical spectrometer was used. It consisted of 1000 channels, with a total bandwidth of 100 MHz and a resolution of 40 KHz, giving velocity resolutions of 0.105 km s⁻¹ at 115 GHz and 0.052 km s⁻¹ at 230 GHz. The system temperatures were ≈ 400 K at 230 GHz and ≈ 320 K at 115 GHz. Pointing was checked once during each observing run on the SiO (*v*=1, *J*=2→1) source VX Sgr. Pointing errors were 3''. The uncertainty in the intensity calibration was 10%. Details about the telescope and receivers can be found in Booth et al. (1989).

The ¹²CO(2-1) and ¹²CO(1-0) data were acquired simultaneously in the position-switching mode on a grid with a spacing of 45''. The off-source position, at which no CO emission was detected, was placed at RA, Dec.(J2000) = (18^h19^m15^s, -11°44'). A total of 143 ¹²CO spectra were taken towards the inner ring and its environs. The observed positions are indicated by crosses on the VLA image (Fig. 1, right panel).

The spectra were reduced using the CLASS software (GILDAS working group)¹. The line intensities are expressed as main-beam brightness temperatures *T_{mb}*, by dividing the antenna temperature *T_A*^{*} by the main-beam efficiency *η_{mb}*, equal to 0.72 and 0.57 at 115 and 230 GHz, respectively (Johansson et al. 1998). The angular resolution of the ¹²CO(2-1) and ¹²CO(1-0) spectra, the velocity range, the original velocity resolution, the velocity resolution after smoothing, and the typical *rms* noise temperatures are listed in Table 3. ¹²CO(2-1) and ¹²CO(1-0) data cubes were constructed using AIPS software.

Complementary ¹²CO(1-0) data obtained with the 4-m NANTEN millimeter-wave telescope of Nagoya University were used to investigate the large scale distribution of the molecular gas in a large area including SerOB2 and the WR star. The half-power beamwidth was 2'.6. The 4K cooled SIS mixer receiver provided typical system temperatures of ≈ 220K (SSB) at this frequency. The acoustical spectrometer (AOS) provided a velocity coverage range of 100 km s⁻¹ and a velocity resolution of 1.0 km/s.

The distribution of the IR emission was analyzed using Spitzer images at 5.6 and 8.0 μm from the Galactic Legacy Infrared Mid-Plane Survey Extraordinaire (Spitzer-GLIMPSE, Benjamin et al. 2003) retrieved from the Spitzer Science Center². Images at 3.4, 4.6, and 12.0 μm with angular resolutions of 6'.1, 6'.5, and 6'.5 from the Wide-field Infrared Survey Explorer (WISE; Wright et al. 2010) were retrieved from IPAC³.

Table 3. Observational parameters of the ¹²CO(1-0) and ¹²CO(2-1) lines observed with SEST.

	¹² CO(2-1)	¹² CO(1-0)
Angular resolution (")	22	45
Velocity range (km s ⁻¹)	(-7,+47)	(-40,+70)
Original velocity resolution (km s ⁻¹)	0.054	0.110
Velocity resolution after smoothing (km s ⁻¹)	0.221	0.332
<i>rms</i> noise (K)	0.17	0.25

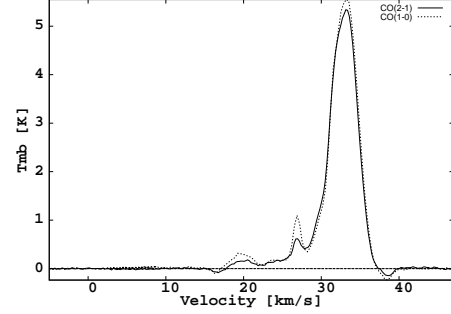


Fig. 2. ¹²CO(2-1) and ¹²CO(1-0) spectra averaged within the surveyed region. Line intensities are expressed as main-beam brightness temperature *T_{mb}*. Velocities are referred to the LSR.

3. The characteristics of the molecular gas

3.1. Spatial distribution

Aimed to detect the molecular gas possibly linked to the ring nebula, we have inspected the data cubes of the ¹²CO(2-1) and ¹²CO(1-0) lines obtained with SEST. The ¹²CO(2-1) and ¹²CO(1-0) spectra averaged within the surveyed region are displayed in Fig. 2. Carbon monoxide emission higher than 5 *rms* is detected between +18 and +37 km s⁻¹. Three molecular components are noticed within the mentioned velocity interval, peaking at ~ +20 km s⁻¹, ~+ 28 km s⁻¹, and +34 km s⁻¹. In Fig. 3 (left panels) we show the spatial distribution of the molecular gas in the velocity ranges from +18.6 to +22.2 km s⁻¹ (Cloud 1), from +25.8 to +28.9 km s⁻¹ (Cloud 2), and from +30 to +36.8 km s⁻¹(Cloud 3) obtained from SEST data. CO intensities are expressed as main-beam brightness temperature averaged within the selected velocity intervals. The cross indicates the position of the WR star. In order to illustrate the large scale distribution of these molecular clouds, the molecular emission in the same velocity ranges as obtained with the NANTEN data is shown in the right panels of Fig. 3, superimposed onto the DSSR image.

Cloud 1 is elongated in the north-south direction with its brightest emission at RA, Dec.(J2000) ~ (18^h18^m50^s, -11°39'). A fainter clump is also detected at RA, Dec.(J2000) ~ (18^h18^m57^s, -11°37'). The NANTEN image shows that this cloud is projected onto the western border of the optical nebula and has a very small angular extension. Using the analytical fit to the circular galactic rotation model of Brand & Blitz (1993) along *l* ≈ 20° we derived for Cloud 1 near and far kinematical distances of about 2 and 14 kpc, respectively. Bearing in mind the lack of morphological agreement with the optical nebula and its small angular size, we believe that Cloud 1 may be a background object, unrelated to the star and the ionized regions. A distance as far as ~ 14 kpc can not be ruled out.

Cloud 2 displays a very clumpy morphology. Although it encircles most of the optical nebula, it shows no clear

¹ <http://www.iram.fr/IRAMFR/PDB/class/class.html>

² <http://sds.spitzer.caltech.edu>

³ <http://www.ipac.caltech.edu>

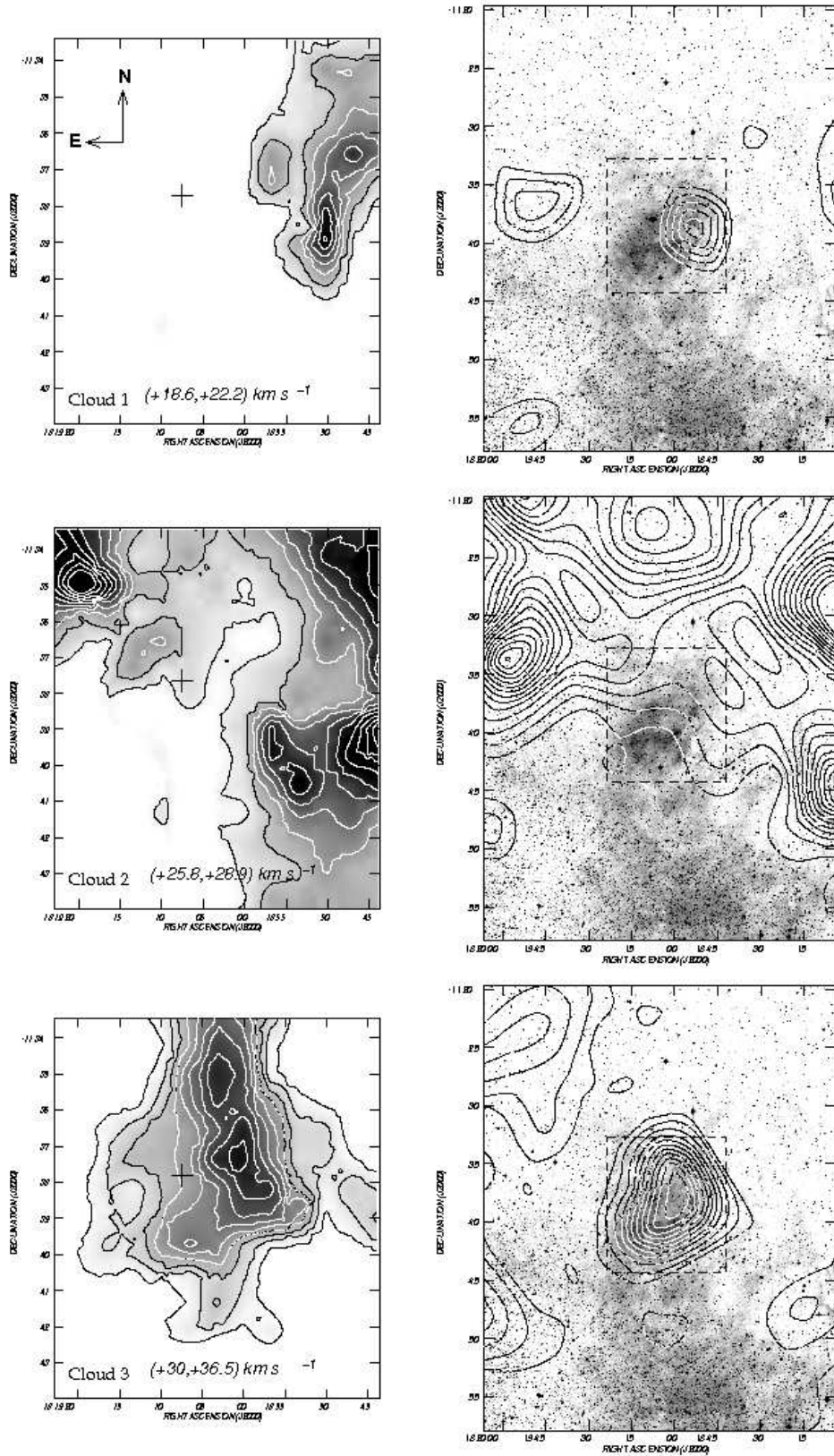


Fig. 3. *Left panels:* ^{12}CO (1-0) emission distribution maps corresponding to Cloud 1 to 3 obtained with the SEST data. For Cloud 1, the grayscale goes from 0.2 to 2 K, and the contour levels are from 0.3 K (~ 4.5 rms) in steps of 0.3 K. For the case of Cloud 2, the grayscale goes from 0.2 to 0.25 K, and the contour levels are from 0.3 K (~ 4 rms) in steps of 0.3 K. For Cloud 3, the grayscale goes from 1 to 8 K, and the contour levels goes from 1 K (~ 20 rms) in steps of 1 K. The cross indicates the position of the WR star. *Right panels:* ^{12}CO (1-0) emission distribution maps corresponding to Clouds 1 to 3 obtained with the NANTEN data (contours), superimposed onto the DSSR image (grayscale). The dashed rectangles at the center of the field indicate the area of the SEST images at the left.

morphological agreement with the ionized gas. Its maxima are present at RA, Dec.(J2000) $\sim (18^h18^m55^s, -11^\circ40')$, RA, Dec.(J2000) $\sim (18^h19^m13^s, -11^\circ37'30'')$, and RA, Dec.(J2000) $\sim (18^h19^m20^s, -11^\circ35')$. Cloud 2 matches with regions lacking optical emission towards the northern, western and southwestern sectors of the nebula. An inspection of the middle right panel of Fig. 3 clearly indicates that Cloud 2 extends well beyond the area surveyed with SEST and NANTEN, which suggests that this cloud is part of a giant molecular cloud (GMC).

The molecular emission of Cloud 3 appears mostly located in the region of the optical nebula. The bulk of the molecular gas is concentrated in an elongated feature extending from between RA, Dec.(J2000) $\sim (18^h19^m05^s, -11^\circ34')$ to RA, Dec.(J2000) $\sim (18^h19^m, -11^\circ39')$. At lower declinations, this feature is shifted toward the east, encircling the position of the WR star. The size and morphology of Cloud 3 is in excellent agreement with the optical nebula. The NANTEN image corresponding to Cloud 3 shows that the bulk of the molecular gas of this cloud coincides with of the optical nebula and does not extend beyond the region surveyed by the SEST data.

The large extent of Cloud 2 and the morphological coincidence with a region lacking optical emission towards the north and west of the nebula speaks in favour of an interpretation in which Cloud 2 is a foreground object with respect to WR 113, or is placed at almost the same distance. On the other hand, the good morphological correspondence of Cloud 3 with the inner optical nebula around WR 113 suggests that this structure is physically related to the ionized ring nebula. It ought to be pointed out that along this galactic longitude, considering mean radial velocities of about $\sim +27.5 \text{ km s}^{-1}$ and $\sim +35.5 \text{ km s}^{-1}$, the galactic velocity field of Brand & Blitz (1993) (see their fig. 2b) along $l \approx 20^\circ$ predicts near kinematical distances of $1.8 \pm 0.5 \text{ kpc}$ and $2.3 \pm 0.5 \text{ kpc}$ for Cloud 2 and Cloud 3, respectively. Uncertainties in these distances were obtained adopting random motions of $\pm 6 \text{ km s}^{-1}$ (Burton & Gordon 1978). Keeping this in mind an interpretation in which Cloud 3 is behind Cloud 2 can not be ruled out. Nevertheless, from the present data we cannot either confirm or deny a physical relation between Cloud 2 and the optical nebula. Based on the above, from here onwards we shall concentrate on the analysis of Cloud 3, which is the only cloud clearly associated with the optical ring nebula around WR 113.

In order to better characterize the kinematical properties of Cloud 3, in Fig. 4 a collection of images depicting the CO(1-0) spatial distribution in the velocity range from $+28.9$ to $+36.9 \text{ km s}^{-1}$ is shown. Every image displays the CO emission averaged over a velocity interval of $\sim 0.9 \text{ km s}^{-1}$ (three individual smoothed channel maps). The CO emission distribution shown in Fig. 4 (in contours) is projected onto the DSSR image of the optical nebula (greyscale). The velocity interval of the individual images is indicated in the lower right corner. In the velocity interval from $+29.8$ to $+32.5 \text{ km s}^{-1}$ the bulk of the molecular emission is concentrated towards the center of the optical nebula and is projected onto the region of relatively faint emission between the stellar position and the bright optical filaments. This coincidence suggests that the faint optical emission observed towards the center of the nebula arises from ionization of photodissociated molecular gas. The VLA image also shows low radio continuum emission in this area, indicating the presence of ionized gas. From $+32.5 \text{ km s}^{-1}$ the molecular gas develops an arc-like morphology, which is better noticed at velocities between $\sim +34.3$ and $+35.2$. This morphology remains at 36.0 km s^{-1} where is still noticed as a hollow patchy annular feature.

3.2. Ratio $R_{2-1/1-0}$ and excitation temperature

A powerful tool that help us to determine the physical conditions of molecular clouds is the $R_{2-1/1-0}$ ratio. Sakamoto et al. (1997) classified the molecular gas in three categories: “very high ratio gas” (VHRG, corresponding to $1.0 < R_{2-1/1-0} < 1.2$), “high ratio gas” (HRG, for $0.7 < R_{2-1/1-0} < 1$), and “low ratio gas” (LRG, for $R_{2-1/1-0} < 0.7$). Values compatible with VHRG denote surfaces of dense clumps irradiated by strong radiation field and PDRs (Gierens et al. 1992). In this case, excitation temperatures (T_{exc}) greater than 50 K and volume densities greater than $3 \times 10^3 \text{ cm}^{-3}$ are expected. Molecular gas with $R_{2-1/1-0} \approx 1.3$ is observed toward HII regions (Castets et al. 1990; Sakamoto et al. 1994), which heat its surrounding molecular dense gas. Ratios in the range 0.7 to 1.0 are usually observed in central regions of giant molecular clouds where CO emission originates in collision processes (Castets et al. 1990, Sakamoto et al. 1994). This material is characterized by $T_{\text{exc}} \gtrsim 20 \text{ K}$ and $n_{\text{H}_2} \gtrsim 1 \times 10^3 \text{ cm}^{-3}$. Finally, $R_{2-1/1-0} < 0.7$ is observed in the outer envelopes of giants molecular clouds. These values are consistent with gas sub-thermally excited, with $T_{\text{exc}} \leq 10 \text{ K}$ and densities $n_{\text{H}_2} < 1 \times 10^3 \text{ cm}^{-3}$. To probe the surface conditions of Cloud 3, we will analyze the T_{exc} -distribution obtained from the CO(1-0) line, assumed to be optically thick.

Fig. 5 shows the spatial distribution of the ratio $R_{2-1/1-0}$ obtained for Cloud 3 in grayscale, where

$$R_{2-1/1-0} = \frac{\int_{v_1}^{v_2} T_{mb(2-1)} dv}{\int_{v_1}^{v_2} T_{mb(1-0)} dv} \quad (1)$$

with $v_1 = 29 \text{ km s}^{-1}$ and $v_2 = 36.5 \text{ km s}^{-1}$. The spatial distribution of $\int_{v_1}^{v_2} T_{mb(2-1)} dv$ and $\int_{v_1}^{v_2} T_{mb(1-0)} dv$ (order-zero moments) were obtained using AIPS package.

The T_{exc} distribution of the ^{12}CO line can be obtained from $T_{\text{peak}}(^{12}\text{CO}) = T^* [J_\nu(T_{\text{exc}}) - J_\nu(T_{bg})]$ (Dickman 1978), where T_{peak} is the peak temperature of the $^{12}\text{CO}(1-0)$ line, $T^* = h\nu/k$, with ν the rest frequency of the $^{12}\text{CO}(1-0)$ line, and $J_\nu(T) = (\exp(T^*/T) - 1)^{-1}$. We adopt a background temperature $T_{bg} \sim 2.7 \text{ K}$. Using this equation, assuming Gaussian profiles for the CO(1-0) line, and combining the order-zero moment map (i.e., integrated areas) with the order-two moment maps (i.e., velocity dispersion), we obtain the T_{exc} distribution map, which is depicted in Fig. 5 with black contours.

An inspection of Fig. 5 shows values of $R_{2-1/1-0}$ between 0.5 and 1.2 along Cloud 3. It is worth to mention that values of $R_{2-1/1-0}$ higher than 1.2 in the border of the CO cloud can not be taken into account due to their large uncertainties. Two small regions at $18^h19^m07^s < \text{RA} < 18^h19^m13^s$ and $-11^\circ37'.5 < \text{DEC} < -11^\circ39'$, and at $18^h19^m05^s < \text{RA} < 18^h19^m12^s$ and $-11^\circ33'.5 < \text{DEC} < -11^\circ35'.5$ exhibit values of $R_{2-1/1-0}$ between ~ 0.4 to ~ 0.7 , probably arising in spots of quiescent dark molecular gas. The rest of the molecular cloud shows higher values (between ~ 0.8 and ~ 1.1), which suggest that the molecular gas of Cloud 3 is being irradiated by an external UV field and might be indicative of the presence of PDRs along Cloud 3. A similar conclusion can be dropped from the T_{exc} -analysis. Excitation temperatures of about $\sim 50 \text{ K}$ are observed towards the brightest part of Cloud 3, which are higher than expected inside molecular cores if only cosmic ray ionization is considered as the main heating source ($T \sim 8 - 10 \text{ K}$, van der Tak & van Dishoeck 2000). Excitation temperatures of about $\sim 30 \text{ K}$ are observed toward molecular clouds located at the edges of evolved HII regions (*bright rimmed clouds*), which implies that additional heating

Table 4. Main physical parameters of Cloud 3.

Parameter	Value
Angular size (′)	~ 7
Linear size (pc)	4.0 ± 1.2
Velocity range (km s ⁻¹)	~ +30, +36
Systemic velocity (km s ⁻¹)	~ 35.5 ± 1.0
H ₂ column density N_{H_2} (10 ²¹ cm ⁻²)	4.1 ± 0.6
Molecular mass M_{H_2} (M _⊙)	~1600 ± 500
n_{H_2} (molecules cm ⁻³)	~ 450

processes, like photoionization, are present close to these clouds (Urquhart et al. 2009). We conclude that Cloud 3 is being externally heated through the photoionisation of its surface layers as a consequence of its proximity to neighbouring ionizing stars.

3.3. Physical parameters of the molecular cloud

Table 4 lists the main physical parameters of Cloud 3, obtained from the ¹²CO(1-0) observations. The table includes angular sizes, velocity ranges, systemic velocities, mean H₂ column densities, and molecular masses. Mean H₂ column densities were derived using the empirical relation between the integrated emission $I_{\text{CO}} (= \int T_{\text{mb}} dv)$ and N_{H_2} . We adopted $N(\text{H}_2) = (1.9 \pm 0.3) \times 10^{20} I_{\text{CO}}$ (cm⁻²) (Digel et al. 1996; Strong & Mattox 1996). The total molecular mass was calculated using $M_{\text{H}_2} = (m_{\text{sun}})^{-1} \mu m_{\text{H}} \sum \Omega N(\text{H}_2) d^2$ (M_⊙), where m_{sun} is the solar mass (~ 2 × 10³³ g), μ is the mean molecular weight, assumed to be equal to 2.8 after allowance of a relative helium abundance of 25% by mass (Yamaguchi et al. 1999), m_{H} is the hydrogen atom mass (~ 1.67 × 10⁻²⁴ g), Ω is the solid angle subtended by the CO feature in ster, and d is the distance. The mean volume density (n_{H_2}) of Cloud 3 can be derived from the ratio of its molecular mass and its volume considering an approximately spherical geometry with a radius of about 2.3 pc.

4. IR counterparts and photodissociated regions

In Fig. 6 we show the mid infrared (MIR) emission at 3.4 μm (blue), 4.6 μm (green), and 12.0 μm (red) in the region of the inner ring nebula. The 3.4 μm and 12 μm filters include prominent PAH emission features and the 4.6 μm filter measures the continuum emission from very small grains (Wright et al. 2010). The emission at 12.0 μm resembles the observed emission at 8.0 μm (see Fig. 1). The emission at 4.6 μm is barely detected towards some stellar sources while the emission at 3.4 and 12 μm delineates clearly the inner optical ring.

Fig. 7 shows the IR emission distribution from the Spitzer-IRAC 8.0 μm image (red), the optical DSS 2R image (blue), and the CO(2-1) contours over a field larger than the region surveyed with SEST. The emission in 8.0 μm, mainly originated in the strong 7.7 and 8.3 μm PAH features, shows a concentration of material along two elongated almost perpendicular regions placed at R.A. ~ 18^h18^m55^s, extending from Decl. ~ -11°40′ to -11°30′, and at Decl. ~ -11°40′, from R.A. ~ 18^h19^m30^s to 18^h18^m50^s. As we described in Section 1.1, the optical inner bright filament appears bordering the MIR emission. Fig. 7 also shows the diffuse optical emission north and south of the inner optical filament. Both emissions, optical and MIR, enclose the molecular cloud towards the south and west.

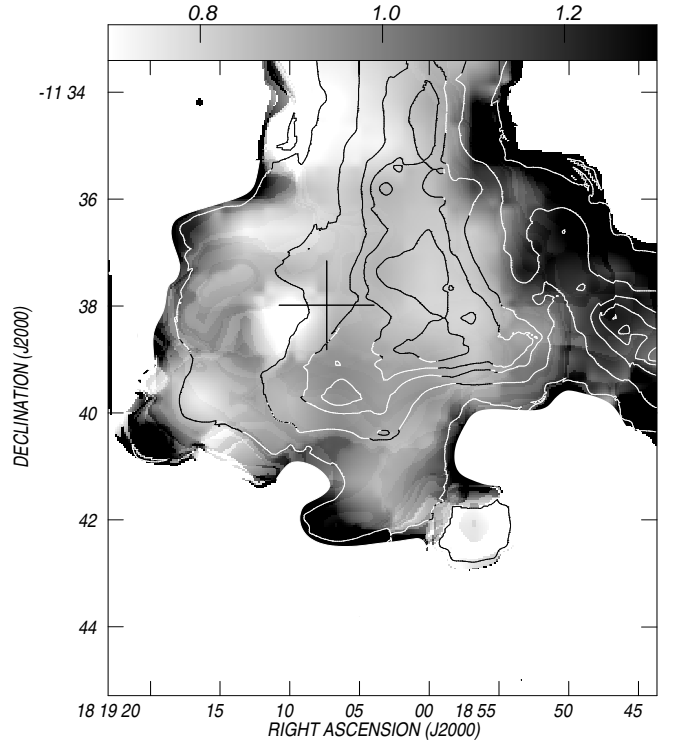


Fig. 5. Line ratios $R_{2-1/1-0}$ for Cloud 3. The grayscale goes from ~ 0.6 (light gray) to ~ 1.3 (dark gray). Black contours correspond to the T_{exc} of the ¹²CO(1-0) line. T_{exc} contours are 10, 20, 30, 35, 40, and 50 K.

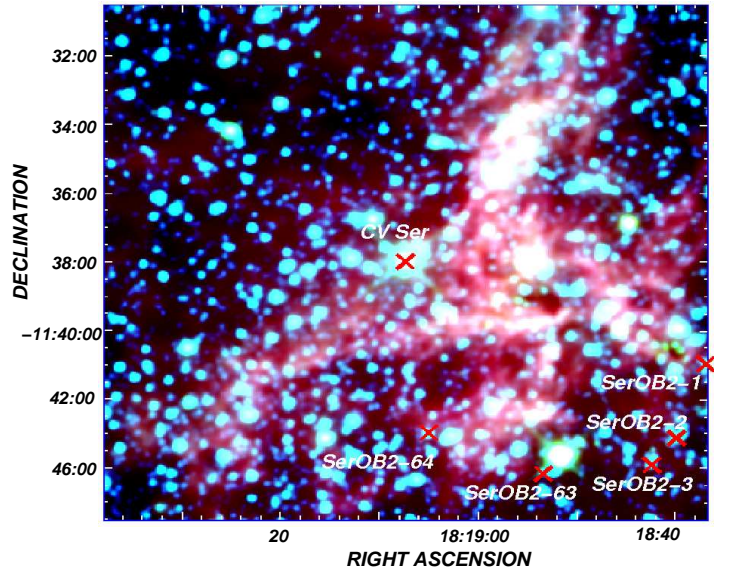


Fig. 6. Superposition of the MIR emissions at 3.4 μm (blue), 4.6 μm (green), and 12.0 μm (red). The positions of WR 113 and the Ser OB2 members are indicated by red crosses.

The presence of PAH emission, which is typical of photodissociation regions (PDRs), at the interphase between the ionized and molecular gas suggests that the molecular gas is being photodissociated by the UV photons emitted by the massive stars (Vasquez et al. 2010). For this reason and according to the morphology of the PAH features observed in Figs. 6 and 7, and the optical and molecular emissions (see Fig. 4), we can confirm

the presence of a PDR located at *Decl.* $\sim -11^\circ 41'$, from *R.A.* $\sim 18^h 18^m 50^s$ to $18^h 19^m 15^s$ which could be generated mainly by the action of the photo-dissociating far-ultraviolet ($6 \text{ eV} < h\nu < 13.6 \text{ eV}$) photons of Ser OB2-1,-2,-3,-63, and -64.

5. Star formation

To investigate the presence of protostellar candidates in the region we used data from the available MSX, 2 MASS, IRAS, and *Spitzer*-IRAC point source catalogs, in a region of about $10'$ in size centered on the position of the WR star.

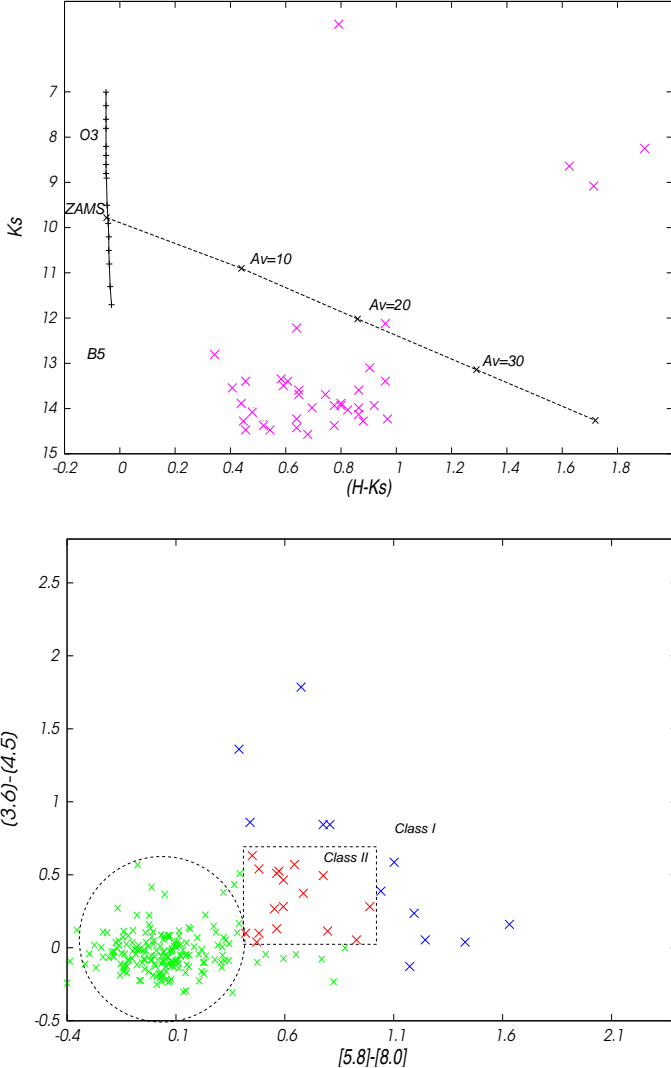


Fig. 8. *Upper panel:* Color-magnitude diagram for the 2MASS sources with IR excess. *Lower panel:* Color-color diagram for the *Spitzer* sources around the region of study.

From an original set of ~ 18000 2 MASS sources, we selected those with high photometrical quality in the J , H , and K_s bands. Following Comerón et al. (2005) we look for candidate YSOs using the parameter $q = (J - H) - 1.83 \times (H - K_s)$. This formula allows one to discriminate between giant and main sequence stars, and sources with IR excess. Sources with $q < -0.15$ are classified as objects with infrared excess, revealing the presence of dusty circumstellar envelopes, i.e. candidate YSOs.

After applying this criterion, we found 39 sources with IR excess. Fig. 8 (upper panel) displays the color-magnitude (CM) diagram of these sources. The ZAMS from O3 to B5 type stars is displayed at the left of the diagram, assuming a distance of 2.0 kpc. Almost all the sources with IR excess present visual absorption larger than 10 mag. Table 3 summarizes the main parameters of these sources, i.e. galactic coordinates, designation, and J , H , and K_s magnitudes.

For the case of IRAS and MSX sources, we search for candidate YSOs following the criteria of Junkes et al. (1992) and Lumsden et al. (2002), respectively. In the case of the IRAS catalog, we do not find any sources satisfying the mentioned criteria into the selected region, while in the case of the MSX catalog, we find only one source at RA, Dec.(J2000) = $(18^h 18^m 56.^s 4, -11^\circ 34' 0.'' 5)$, candidate to compact HII region.

In order to complete the search for candidate YSOs around the optical nebula, we use the GLIMPSE 3D (2007-2009) catalog to perform a photometric study in the region. Considering only sources detected in the four *Spitzer*-IRAC bands, we found 8477 sources. To investigate the evolutionary stage of these sources, we have analyzed their location in a color-color diagram (Fig. 8, lower panel), following the color criteria from Allen et al. (2004). As expected, most of sources seem to cluster around (0,0). This region of the diagram contain mostly background/foreground stars and Class III sources with no intrinsic IR excess. Sources in red occupy the Class II region ($0 \leq [3.6]-[4.5] \leq 0.7$, $0.4 \leq [5.8]-[8.0] \leq 1$), and their IR excess might be produced by accretion disks around the stellar object. Sources in the domain of Class I objects ($0.7 \leq [3.6]-[4.5]$, $1 \leq [5.8]-[8.0]$) are displayed in blue. In this case, the IR excess originates in circumstellar envelopes around the young stellar object.

In Fig.7 we display the position of the candidate YSOs mentioned above. Many of them are projected outside Cloud 3, which suggests that these sources are background/foreground objects unrelated to the region of study. Among the candidate YSOs projected onto Cloud 3, 22 are 2MASS sources, while only six and four are Class I and Class II, respectively. Unlike the 2MASS sources, which are spread onto Cloud 3, Class I and Class II sources appear concentrated in two spots near RA, Dec.(J2000) = $(18^h 18^m 52^s, -11^\circ 38' 45'')$. This location is almost coincident with a region of high optical absorption and a clump of molecular gas better noticed at velocities between $+33.4$ and $+35.2 \text{ km s}^{-1}$ (see Fig. 4). This coincidence shows clearly that star formation is active in this region. The small value of the molecular mass ($\sim 1600 M_\odot$) suggests that this cloud is the remnant of a larger parental cloud that has been photoionized and dissociated by the emerging young stars. To investigate whether these candidate Class I and Class II sources may have been triggered by the expansion of the molecular gas in a “collect and collapse” scenario we applied the analytical model of Whitworth et al. (1994). According to this model expanding nebulae compress gas between the ionization and the shock fronts, leading to the formation of molecular cores where new stars can be embedded. Using the Whitworth et al.’s formulae for the case of expanding HII regions, we derived the time when the fragmentation may have occurred, t_{frag} , and the size of the HII region at t_{frag} , R_{frag} , which are given by $t_{frag}[10^6 \text{ yr}] = 1.56 a_2^{4/11} n_3^{-6/11} N_{49}^{-1/11}$ and $R_{frag}[pc] = 5.8 a_2^{4/11} n_3^{-6/11} N_{49}^{1/11}$, where a_2 is the sound velocity in units of 0.2 km s^{-1} , $n_3 \equiv n_{H_2}/1000$, and $N_{49} \equiv N_{Lyc}^*/10^{49}$. Adopting 0.3 km s^{-1} for the sound velocity (corresponding to temperatures of 3050 K in the surrounding molecular clouds), we obtained $t_{frag} \sim 1.2 \times 10^6 \text{ yr}$,

and $R_{\text{frag}} \sim 15$ pc. Considering that t_{frag} and R_{frag} are higher than the dynamical age of Cloud 3 ($t_{\text{dyn}} \sim 1.0 \times 10^5$ yr; see Sect 6) and its radius ($R_{\text{cloud 3}} \sim 2.3$ pc) we conclude that the fragmentation at the edge of Cloud 3 is doubtful. Nevertheless, the clustered aspect of these sources make them excellent candidates for investigating star formation with high angular resolution observations.

6. Scenario

As mentioned in Section 1.1, Gonzalez & Rosado (1984) and Esteban & Rosado (1995) (using optical lines), and Cappa et al. (2002) (using radio continuum data), explained the inner optical bright filament and its radio counterparts as the result of action of the UV field and the strong stellar winds of the star WR 113. An alternative scenario can be proposed taking into account the kinematical properties of Cloud 3, and the location of the WR star and SerOB2-1, -2, -3, -63, and -64.

Along the velocity interval from $+32.5$ to $+36$ km s⁻¹, WR 113 appears projected onto a region of faint molecular emission, which suggests that the star is interacting with the molecular cloud. The relatively large velocity range of Cloud 3 (~ 7 km s⁻¹) suggests that expanding motions are present in the molecular gas. The classical wind-blown expanding shell scenario predicts that the surrounding gas expands spherically around the star. Then, if the molecular emission is a two-dimensional projection of an expanding spherical shell, it should appear in the data cube first as a blueshifted pole (approaching cap), then as a growing-decreasing circular ring, and finally as a redshifted pole (receding cap), with the powering star placed at the center or close to it. According to Fig. 4, the approaching section of this shell is present, although the receding part is missed. Note also that the brightest optical ring coincides with the outer border of Cloud 3, indicating that this cloud is also being photodissociated by an external source, possibly located towards the southwest. Bearing in mind the location of SerOB-1, -2, -3, -63 and -64 (see Table 2) and their linear distance to Cloud 3 (1 - 2 pc, taking into account a distance of 2.0 kpc), we speculate that these stars are responsible for the inner optical ring. The diffuse optical emission observed north of the bright optical ring, in the region between $18^{\text{h}}18^{\text{m}}50^{\text{s}} < \text{RA} < 18^{\text{h}}19^{\text{m}}20^{\text{s}}$ and $-11^{\circ}36' < \text{DEC} < -11^{\circ}40'$ might arise from the photodissociation of the molecular gas at the surface of Cloud 3 that faces the Earth, probably at lower radial velocities (between $+30$ and $+32$ km s⁻¹), since we indeed detect optical emission. The diffuse optical emission at the south of the optical rim, between $-11^{\circ}40' < \text{DEC} < -11^{\circ}42'$ probably originates in the dissociation of the small molecular clump at RA, Dec.(J2000) = ($18^{\text{h}}19^{\text{m}}3^{\text{s}}, -11^{\circ}41'30''$), with velocities between $+34.3$ and $+36.0$ km s⁻¹.

In Fig. 9 we present a side view of a simple sketch of the scenario proposed to explain the characteristics of the molecular and ionized gas. Cloud 3 is a half-shell which expands around CV Ser as the result of the wind mechanical energy injected into the ambient medium by the binary system. The stars SerOB2-1, -2, -3, -63, and -64, belonging to SerOB2, photodissociate and ionize the southern and central region of the outer face of Cloud 3 giving rise to the diffuse emission observed at optical wavelengths. According to this scenario, the intensity of the optical emission is expected to rise as the thickness of the emitting ionized region in the line of sight increases. Then, the maximum of the optical emission should be observed toward the edge of the molecular cloud (*limb brightening*), which explain the location of the inner optical ring at the southern and western borders of

Cloud 3 (see Fig. 9). The PAH emission is originated in the PDR at the interface between the ionized and molecular gas. The UV field of CV Ser ionizes the inner face of Cloud 3, although the optical emission is probably mostly absorbed by the dust linked to the molecular gas in the line of sight.

We estimated an expansion velocity, $V_{\text{exp}} = 6$ km s⁻¹. Similar expansion velocity values were derived for the expanding shells linked to WR stars, e.g. ~ 7.4 km s⁻¹ (Vasquez et al. (2009)), ~ 9 km s⁻¹ (Cappa et al. (2009)), 8 ± 1 km s⁻¹ (Vasquez et al. (2010)). Adopting an expansion velocity of 6 km s⁻¹, the dynamical age of the half-shell, according to wind blown bubble models can be calculated using $t_{\text{dyn}} = 0.5 \times 10^6 \times \frac{R}{V_{\text{exp}}}$ (McCray 1983; Howarth & Lamers 1999), where R is the radius of the bubble (pc). We obtain $t_{\text{dyn}} \approx 2 \times 10^5$ yr, which is in agreement, within the errors, with the dynamical age obtained by Cappa et al. (2002) using radio continuum data.

From the value of the molecular mass and the expansion velocity, we determined a kinetic energy $E_{\text{kin}} = 6 \times 10^{47}$ erg and a momentum $P = 9.6 \times 10^3 M_{\odot}$ km s⁻¹ for the molecular cloud. To calculate the mechanical energy injected by CV Ser, we shall assume typical values for the stellar wind of a WC 8 star ($\dot{M} = 2.5 \times 10^{-5} M_{\odot}$ yr⁻¹, $v_{\infty} = 1890$ km s⁻¹; Nugis & Lamers 2000), and for its O9V type star companion ($\dot{M} = 4.0 \times 10^{-6} M_{\odot}$ yr⁻¹ and $v_{\infty} = 1800$ km s⁻¹; Smith et al. 2002). We obtain for CV Ser a mechanical luminosity of $L_w \approx 3.2 \times 10^{37}$ erg s⁻¹. Considering a lifetime for the binary system equal to the age of SerOB2 (5×10^6 yr; Forbes 2000), the mechanical energy injected by the binary system into the interstellar medium is $E_w \approx 5.1 \times 10^{51}$ erg. Thus, the energy conversion efficiency is $\frac{E_{\text{kin}}}{E_w} \sim 0.01\%$. In other words, only a small fraction of the mechanical energy released by CV Ser is needed to account for the kinetic energy of the expanding molecular gas. It is useful to stress that conversion efficiencies of the order of 2-5 % were reported in interstellar bubbles (Cappa et al. 2001; Cichowolski et al. 2001, 2003; Cappa et al. 2009). Further, theoretical models and numerical simulations also suggest that in wind bubbles only a few percent of the injected mechanical energy will be converted into kinetic energy of the expanding gas (Weaver et al. 1977; Koo & McKee 1992; Arthur 2007).

The derived values of energy conversion efficiencies are similar to estimates for other stellar wind bubbles (e.g., Cappa 2006). They are in agreement with predictions from recent numerical simulations from Freyer et al. 2003 and (Freyer et al. 2006). The analysis by Freyer et al. takes into account the action of the stellar wind and the ionizing flux from stars of 35 and 60 M_{\odot} and find that $\frac{E_{\text{kin}}}{E_w}$ is in the range 0.10-0.04. In addition, according to our model Cloud 3 subtends a small solid angle ($\leq 2\pi$) which reduces the wind mechanical energy available to it. Based on the above derived figures and considerations, the stellar winds of CV Ser are very capable of providing the kinetic energy of Cloud 3. Similarly, the momentum injected by the strong stellar wind of CV Ser to the ISM, taking into account \dot{M} , v_{∞} for the binary system is $P_{\text{CVSer}} \approx 2.7 \times 10^5 M_{\odot}$ km s⁻¹, which yields to a conversion efficiency $\frac{P}{P_{\text{CVSer}}} \sim 4\%$. The estimated value corresponds neither to the energy nor to the momentum conserving models. We believe that the existence of the approaching molecular shell strongly affects the energy and momentum efficiencies.

7. Summary

With the aim of investigating the molecular gas around CV Ser and better understand the interstellar scenario in the environs of the binary system, we analysed SEST ¹²CO($J = 1 - 0$) (HPBW

= 44") and ($J = 2 - 1$) (HPBW = 22") data, and complementary NANTEN $^{12}\text{CO}(1-0)$ data. The MIR data at 4.5 to 12 μm , along with *Spitzer* images allowed us to make a more comprehensive study of the dust around the nebula.

The more important aspects of this study can be summarized as follows:

- A molecular cloud in the velocity interval from $\sim +30$ to $+37 \text{ km s}^{-1}$ (Cloud 3) was found to be associated with the optical ring nebula around the binary system CV Ser. Morphological and kinematical properties indicate that this cloud is a half shell expanding around CV Ser.
- The strong stellar winds of CV Ser are the main responsables for shaping and for the kinematics of the molecular shell.
- The inner optical ring is placed along the outer edge of the molecular cloud. This suggests that the stars Ser OB2-1, -2, -3, -63 and -64, belonging to Ser OB2 and located 1 - 2 pc far from Cloud 3, ionize the outer face of the molecular cloud originating the optical ring nebula and the diffuse optical emission observed towards the center of the cloud. The observed PDR located between the molecular cloud and the ionized gas is also generated by the action of these stars.
- A collection of candidate YSOs are detected towards the molecular cloud. Two small clusters of Class I and Class II objects are projected onto a region of high optical absorption, coincident with a small clump of molecular gas, indicating that star formation is active in this region. Although analytical models indicate that a triggered star formation scenario is **doubtful** more studies are necessary to shed some light on this issue .

Acknowledgements. We acknowledge the anonymous referee of her/his comments. J.V. acknowledges the hospitality of the Astronomy Department of Universidad de Chile during his stay in Santiago, Chile. We are grateful to Dr. N. Mizuno for providing us the NANTEN data. This project was partially financed by CONICET of Argentina under project PIP 2488/09, UNLP under project 11/G093, and ANPCyT under project PICT 903/08. M.R. is supported by the Chilean Center for Astrophysics FONDAF No. 15010003. M.R. wishes to acknowledge support from FONDECYT (Chile) grant No. 1080335.

This research has made use of the NASA/ IPAC Infrared Science Archive, which is operated by the Jet Propulsion Laboratory, California Institute of Technology, under contract with the National Aeronautics and Space Administration. This publication makes use of data products from the Two Micron All Sky Survey, which is a joint project of the University of Massachusetts and the Infrared Processing and Analysis Center/California Institute of Technology, funded by the National Aeronautics and Space Administration and the National Science Foundation.

References

Allen, L. E., Calvet, N., D'Alessio, P., et al. 2004, *ApJS*, 154, 363
 Arthur, S. J. 2007, *Wind-Blown Bubbles around Evolved Stars*, ed. Hartquist, T. W., Pittard, J. M., & Falle, S. A. E. G., 183
 Benjamin, R. A., Churchwell, E., Babler, B. L., et al. 2003, *PASP*, 115, 953
 Booth, R. S., Delgado, G., Hagstrom, M., et al. 1989, *A&A*, 216, 315
 Brand, J. & Blitz, L. 1993, *A&A*, 275, 67
 Burton, W. B. & Gordon, M. A. 1978, *A&A*, 63, 7
 Cappa, C., Niemela, V. S., Martín, M. C., & McClure-Griffiths, N. M. 2005, *A&A*, 436, 155
 Cappa, C. E. 2006, in *Revista Mexicana de Astronomía y Astrofísica Conference Series*, Vol. 26, *Revista Mexicana de Astronomía y Astrofísica Conference Series*, 9–12
 Cappa, C. E., Goss, W. M., & Pineault, S. 2002, *AJ*, 123, 3348
 Cappa, C. E., Rubio, M., & Goss, W. M. 2001, *AJ*, 121, 2664
 Cappa, C. E., Rubio, M., Martín, M. C., & Romero, G. A. 2009, *A&A*, 508, 759
 Castets, A., Duvert, G., Dutrey, A., et al. 1990, *A&A*, 234, 469

Chu, Y. H. 1991, in *IAU Symposium*, Vol. 143, *Wolf-Rayet Stars and Interrelations with Other Massive Stars in Galaxies*, ed. K. A. van der Hucht & B. Hidayat, 349
 Cichowolski, S., Arnal, E. M., Cappa, C. E., Pineault, S., & St-Louis, N. 2003, *MNRAS*, 343, 47
 Cichowolski, S., Pineault, S., Arnal, E. M., et al. 2001, *AJ*, 122, 1938
 Comerón, F., Schneider, N., & Russeil, D. 2005, *A&A*, 433, 955
 Conti, P. S., Ebbets, D., Massey, P., & Niemela, V. S. 1980, *ApJ*, 238, 184
 Conti, P. S. & Vacca, W. D. 1990, *AJ*, 100, 431
 Dickman, R. L. 1978, *ApJS*, 37, 407
 Digel, S. W., Grenier, I. A., Heithausen, A., Hunter, S. D., & Thaddeus, P. 1996, *ApJ*, 463, 609
 Esteban, C. & Rosado, M. 1995, *A&A*, 304, 491
 Forbes, D. 2000, *AJ*, 120, 2594
 Freyer, T., Hensler, G., & Yorke, H. W. 2003, *ApJ*, 594, 888
 Freyer, T., Hensler, G., & Yorke, H. W. 2006, *ApJ*, 638, 262
 Gierens, K. M., Stutzki, J., & Winnewisser, G. 1992, *A&A*, 259, 271
 Gonzalez, J. & Rosado, M. 1984, *A&A*, 134, L21
 Goss, W. M. & Day, G. A. 1970, *Australian Journal of Physics Astrophysical Supplement*, 13, 3
 Howarth, I. & Lamers, H. J. G. 1999, *Journal of the British Astronomical Association*, 109, 347
 Johansson, L. E. B., Greve, A., Booth, R. S., et al. 1998, *A&A*, 331, 857
 Junkes, N., Fuerst, E., & Reich, W. 1992, *A&A*, 261, 289
 Koesterke, L. & Hamann, W.-R. 1995, *A&A*, 299, 503
 Koo, B.-C. & McKee, C. F. 1992, *ApJ*, 388, 93
 Lamontagne, R., Moffat, A. F. J., Drissen, L., Robert, C., & Matthews, J. M. 1996, *AJ*, 112, 2227
 Leitherer, C., Chapman, J. M., & Koribalski, B. 1997, *ApJ*, 481, 898
 Leitherer, C., Forbes, D., Gilmore, A. C., et al. 1987, *A&A*, 185, 121
 Lockman, F. J. 1989, *ApJS*, 71, 469
 Lumsden, S. L., Hoare, M. G., Oudmaijer, R. D., & Richards, D. 2002, *MNRAS*, 336, 621
 Massey, P. & Niemela, V. S. 1981, *ApJ*, 245, 195
 McCray, R. 1983, *Highlights of Astronomy*, 6, 565
 Mueller, P., Reif, K., & Reich, W. 1987, *A&A*, 183, 327
 Nugis, T., Crowther, P. A., & Willis, A. J. 1998, *A&A*, 333, 956
 Nugis, T. & Lamers, H. J. G. L. M. 2000, *A&A*, 360, 227
 Sakamoto, S., Hasegawa, T., Handa, T., Hayashi, M., & Oka, T. 1997, *ApJ*, 486, 276
 Sakamoto, S., Hayashi, M., Hasegawa, T., Handa, T., & Oka, T. 1994, *ApJ*, 425, 641
 Smith, L. J., Norris, R. P. F., & Crowther, P. A. 2002, *MNRAS*, 337, 1309
 Strong, A. W. & Mattox, J. R. 1996, *A&A*, 308, L21
 Urquhart, J. S., Morgan, L. K., & Thompson, M. A. 2009, *A&A*, 497, 789
 van der Hucht, K. A. 2001, *New A Rev.*, 45, 135
 van der Tak, F. F. S. & van Dishoeck, E. F. 2000, *A&A*, 358, L79
 Vasquez, J., Cappa, C. E., & Pineault, S. 2009, *MNRAS*, 395, 2045
 Vasquez, J., Cappa, C. E., Pineault, S., & Duronea, N. U. 2010, *MNRAS*, 405, 1976
 Weaver, R., McCray, R., Castor, J., Shapiro, P., & Moore, R. 1977, *ApJ*, 218, 377
 Whitworth, A. P., Bhattal, A. S., Chapman, S. J., Disney, M. J., & Turner, J. A. 1994, *A&A*, 290, 421
 Wright, E. L., Eisenhardt, P. R. M., Mainzer, A. K., et al. 2010, *AJ*, 140, 1868
 Yamaguchi, N., Mizuno, N., Saito, H., et al. 1999, *PASJ*, 51, 775

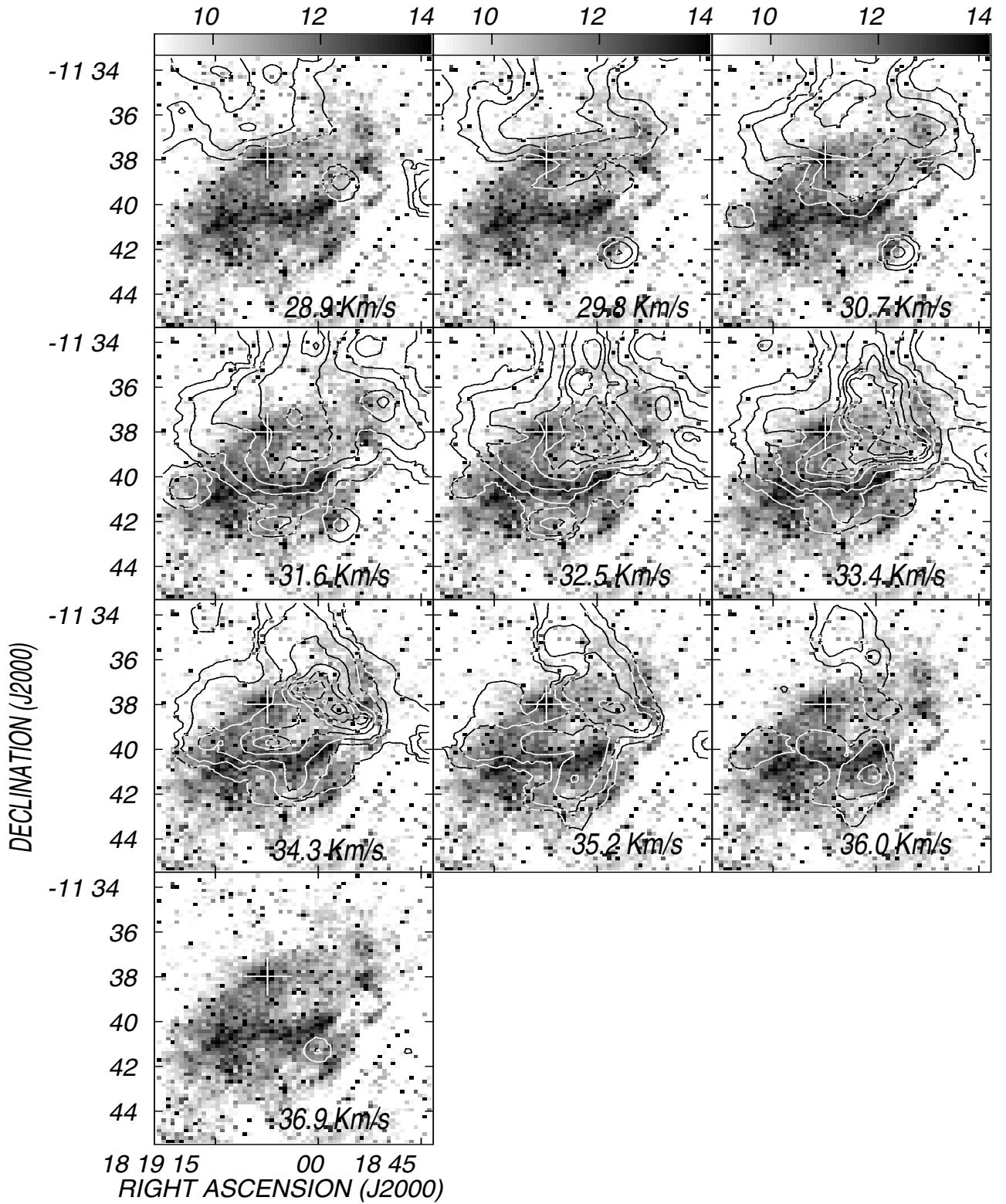


Fig. 4. Overlay of the mean CO emission (contours) in the velocity range from 28.9 to 36.9 km s⁻¹ and the DSSR emission of the optical nebula (grayscale). The central velocity is indicated in the lower right corner of each image. Contour levels are 1, 2, 4, 8, 11, 13, and 15 K. The position of WR 113 is indicated with the white cross.

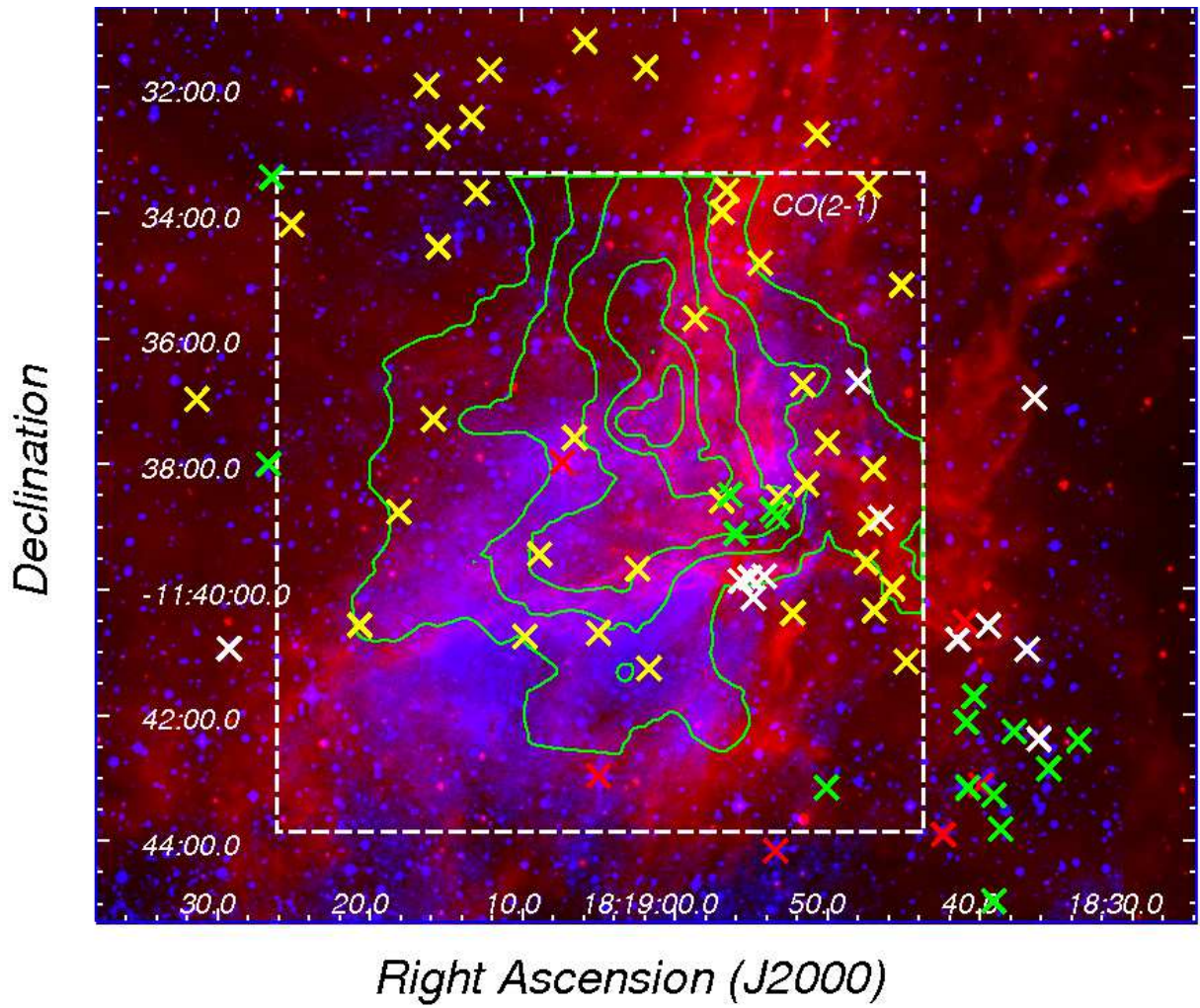


Fig. 7. Overlay of the $8\mu\text{m}$ -image (in red), the optical (DSS2 R, in blue), and millimetre (CO(2-1), green contours) images of the region. The yellow crosses indicate the position of the 2 MASS point sources with IR excess, while the white and green crosses indicate the IRAC class I and class II sources, respectively. Finally, the red crosses indicate the position of CV Ser and Ser OB-1,-2,-3,-63 and -64.

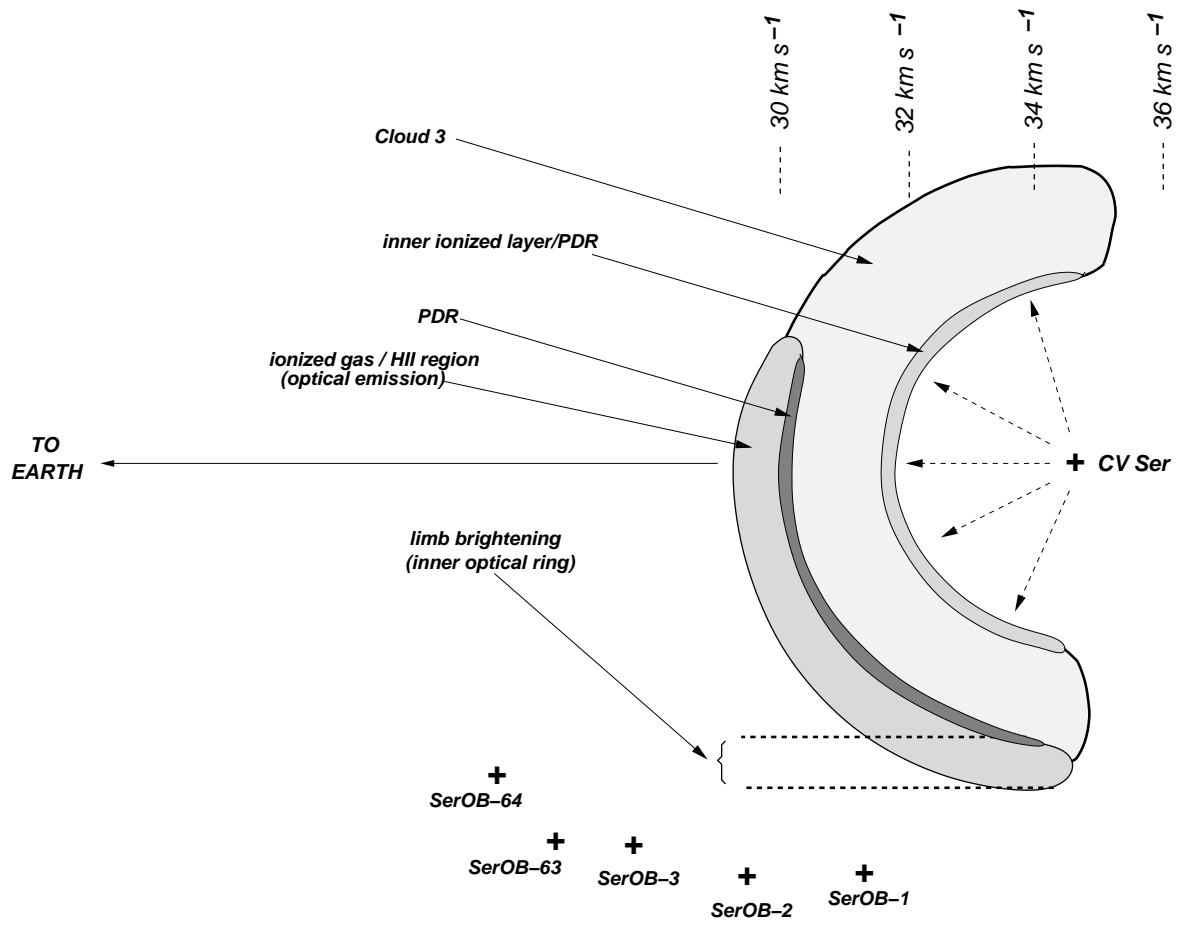


Fig. 9. Sketch of the model used to explain the characteristics of the molecular and ionized gas.

Table 3. YSO candidates projected over the region.

2MASS						
Name	RA, Dec.(J2000)	<i>J</i> [mag]	<i>H</i> [mag]	<i>K_s</i> [mag]		
18190736-1137591	18:19:7	-11:37:59.1312	7.016	6.283	5.492	
18190884-1139265	18:19:8	-11:39:26.5932	15.859	14.684	13.888	
18185686-1134000	18:18:56	-11:34:0.0192	13.448	10.152	8.255	
18185863-1135413	18:18:58	-11:35:41.3448	14.492	13.956	13.547	
18190584-1131161	18:19:5	-11:31:16.1292	16.194	15.234	14.556	
18185132-1138198	18:18:51	-11:38:19.8348	14.913	13.997	13.395	
18184741-1139346	18:18:47	-11:39:34.668	14.347	11.825	9.379	
18185437-1134484	18:18:54	-11:34:48.4104	15.831	14.457	13.591	
18185653-1133388	18:18:56	-11:33:38.808	16.310	14.856	13.937	
18191623-1131588	18:19:16	-11:31:58.8	15.439	14.014	13.106	
18191547-1132478	18:19:15	-11:32:47.832	15.336	14.708	14.256	
18191209-1131439	18:19:12	-11:31:43.9248	13.528	13.162	12.820	
18184689-1140203	18:18:46	-11:40:20.37	16.275	15.167	14.198	
18191326-1132294	18:19:13	-11:32:29.4576	16.161	14.827	13.961	
18191548-1134327	18:19:15	-11:34:32.7216	15.955	14.709	13.938	
18184570-1139594	18:18:45	-11:39:59.4864	13.532	10.775	9.065	
18190241-1139407	18:19:2	-11:39:40.7556	13.711	12.860	12.218	
18190655-1137351	18:19:6	-11:37:35.148	14.757	13.902	13.322	
18192507-1134108	18:19:25	-11:34:10.8876	12.806	10.280	8.657	
18184479-1141092	18:18:44	-11:41:9.2148	15.483	14.647	13.955	
18185316-1138319	18:18:53	-11:38:31.9632	15.598	14.851	14.331	
18184510-1135094	18:18:45	-11:35:9.4632	14.612	13.099	12.139	
18191292-1133406	18:19:12	-11:33:40.6296	14.524	13.864	13.407	
18185691-1138354	18:18:56	-11:38:35.4084	14.700	14.329	13.891	
18184716-1138575	18:18:47	-11:38:57.5988	15.651	14.994	14.453	
18193130-1136578	18:19:31	-11:36:57.8808	15.991	15.031	14.388	
18190185-1131418	18:19:1	-11:31:41.8692	16.039	15.142	14.363	
18190169-1141155	18:19:1	-11:41:15.5688	15.338	14.318	13.671	
18184726-1133344	18:18:47	-11:33:34.4772	15.087	14.519	14.044	
18191809-1138460	18:19:18	-11:38:46.0824	15.443	14.408	13.668	
18185062-1132452	18:18:50	-11:32:45.294	16.203	15.118	14.242	
18184694-1138052	18:18:46	-11:38:5.2584	15.518	14.927	14.469	
18185224-1140231	18:18:52	-11:40:23.1708	14.921	14.073	13.484	
18190983-1140452	18:19:9	-11:40:45.228	16.219	14.999	14.138	
18184996-1137399	18:18:49	-11:37:39.9936	15.938	14.338	13.379	
18191577-1137174	18:19:15	-11:37:17.4504	15.883	14.867	14.223	
18185159-1136448	18:18:51	-11:36:44.8344	15.644	14.755	13.955	
18190499-1140419	18:19:4	-11:40:41.9808	15.997	14.832	14.012	
18192064-1140341	18:19:20	-11:40:34.1004	15.215	14.217	13.566	
IRAC (Class I)						
Name	RA, Dec.(J2000)	[3.6] [mJy]	[4.5] [mJy]	[5.8] [mJy]	[8.0] [mJy]	
G018.8888+01.8312	18:18:47	-11:36:41.6088	1.389000	0.923700	2.600000	5.412000
G018.8152+01.8312	18:18:39	-11:40:34.9572	4.999000	6.915000	9.280000	10.660000
G018.8190+01.8261	18:18:40	-11:40:31.3932	2.304000	5.135000	10.280000	8.187000
G018.8158+01.8223	18:18:41	-11:40:48.1116	8.123000	11.270000	15.860000	18.620001
G018.8550+01.7845	18:18:54	-11:39:48.0924	19.340000	15.520000	26.340000	43.950001
G018.8514+01.7792	18:18:54	-11:40:8.3856	0.895400	1.261000	2.747000	2.281000
G018.8540+01.8193	18:18:46	-11:38:52.0728	4.180000	3.822000	4.604000	6.690000
G018.8626+01.8707	18:18:36	-11:36:57.4668	2.881000	9.610000	20.260000	21.110001
G018.8565+01.7810	18:18:55	-11:39:49.2012	2.993000	2.224000	6.030000	15.150000
G018.8569+01.7784	18:18:55	-11:39:52.3584	3.836000	2.565000	4.646000	8.199000
G018.7823+01.8288	18:18:36	-11:42:23.4252	5.035000	5.525000	6.159000	9.447000
G018.9059+01.6493	18:19:29	-11:40:56.3916	1.625000	0.925700	1.329000	2.185000
IRAC (Class II)						
G018.7887+01.7997	18:18:43	-11:42:52.6608	11.310000	10.780000	10.240000	8.016000
G018.7500+01.7978	18:18:39	-11:44:58.5132	1.633000	1.678000	1.464000	1.380000
G018.8687+01.7831	18:18:55	-11:39:6.9192	6.715000	7.711000	9.600000	8.156000
G018.7872+01.8240	18:18:37	-11:42:16.1028	3.466000	3.565000	3.959000	3.744000
G018.7660+01.8084	18:18:38	-11:43:49.5444	12.800000	12.590000	11.850000	11.430000
G018.7741+01.8274	18:18:35	-11:42:51.7788	3.781000	3.821000	3.752000	4.299000
G018.7748+01.8111	18:18:39	-11:43:17.2596	1.671000	1.770000	1.929000	1.675000
G018.7760+01.7794	18:18:46	-11:44:7.3068	2.620000	2.677000	2.298000	1.841000
G018.7769+01.8381	18:18:33	-11:42:24.696	2.354000	2.556000	2.122000	2.144000
G018.9792+01.7830	18:19:80	-11:33:16.7724	10.160000	9.544000	5.075000	2.799000
G018.7823+01.8288	18:18:36	-11:42:23.4252	5.035000	5.525000	6.159000	9.447000
G018.7723+01.7188	18:18:58	-11:46:2.0496	2.182000	2.357000	1.775000	0.922700